Variability Study of MWCNT Local Interconnects Considering Defects and Contact Resistances - Part II: Impact of Charge Transfer Doping

Rongmei Chen, Jie Liang, Jaehyun Lee, Vihar P. Georgiev, Raphael Ramos, Hanako Okuno, Dipankar Kalita, Yuanqing Cheng, Liuyang Zhang, Reetu Raj Pandey, et al.

Variability Study of MWCNT Local Interconnects Considering Defects and Contact Resistances – Part II: Impact of Charge Transfer Doping

Rongmei Chen, Jie Liang, Jaehyun Lee, Vihar P. Georgiev, Raphael Ramos, Hanako Okuno, Dipankar Kalita, Yuanqing Cheng, Liuyang Zhang, Reetu R. Pandey, Salvatore Amoroso, Campbell Millar, Asen Asenov, Jean Dijon, Aida Todri-Sanial

***Abstract*—In this paper, the impact of charge transfer doping on the variability of MWCNT local interconnects is studied by experiments and simulations. We calculate the number of conducting channels of both metallic and semiconducting CNTs as a function of Fermi level shift due to doping based on the calculation of transmission coefficients. By using the MWCNT compact model proposed in Part I of this paper, we study the charge transfer doping of MWCNTs employing Fermi level shift to reduce the performance variability due to changes in diameter, chirality, defects and contact resistance. Simulation results show that charge transfer doping can significantly improve MWCNT interconnect performance and variability by increasing the number of conducting channels of shells and degenerating semiconducting shells to metallic shells. As a case study on a MWCNT of 11 nm outer diameter, when the Fermi level shifts to 0.1 eV, up to ∼80% of performance and standard deviation improvements are observed. Furthermore, a good match between experimental data and simulation results is observed, demonstrating the effectiveness of doping, the validity of the MWCNT compact model and proposed simulation methodology.**

***Index Terms*—multi-walled carbon nanotubes, charge transfer doping, defects, Fermi level, variability, Monte Carlo simulation.**

I. Introduction

As an alternative back-end-of-line material, carbon nanotubes (CNTs) present a viable opportunity due to their ballistic transport, high thermal conductivity, and ampacity [1], [2]. Compared to copper lines, CNTs are more resilient and immune to electromigration (EM) as they can sustain significantly larger current densities than Cu [3]. Furthermore, the resistance of CNT interconnects can be reduced by applying doping such as charge transfer internal or external doping. Doping improves CNT conductivity through the Fermi level, E_f shift to increase the density of charge carriers (by either holes for p-type doping or electrons for n-type doping) [4]–[7]. It was also experimentally demonstrated that doping could improve CNT conductivity regardless of CNT diameter and type (either metallic or semiconducting) as in [4]. In [8], it was shown that the addition of MoOx, which forms a composite material with CNT, makes the improved conductivity of doped CNT stable in air at the temperatures up to 390 ^{o}C. Similar stable doping has also been achieved by utilizing a single electron oxidant to efficiently dope CNT films by [9].

The shift of E_f of CNT can be controlled or tuned by chemical (alkali metals, acids, halogens, ...) [10] or electrochemical doping [11]. In theory, the E_f of semiconducting CNT is at the equipotential position between the conduction and valence band, obtaining p-type and n-type doping with electron-borrowing and donating effects, respectively. Generally, the doping procedure involves the immersion of CNTs into a concentrated solution of dopant for a period of time or exposure to an atmosphere for gaseous dopants [7]. Depending on either the electronegativity for atomic dopants or the electrochemical potential for molecules and inorganic materials, p- or n-type dopants can be achieved. Due to reactions with the oxygen in the air under ambient conditions, CNTs are slightly p-doped. Therefore p-type doping of CNTs is more efficient and practical to improve CNT electrical properties. There are many kinds of p-type dopants, including NO_2 [12], H_2SO_4 and $SOCl_2$ [13], and the combination of HNO_3 and $SOCl_2$ [14], etc. [7]. Recently, iodine [15] , MoO_3 [16] and $PtCl_4$ [17] based p-type charge transfer doping have been presented. Charge transfer doping is based on Van der Waals interaction. Compared to substitutional doping, where the covalent bonding between carbon and external atoms forms a bamboo-like morphology [18], the charge transfer doping does not modify the CNT structure and hence reduces morphological defects and avoids unexpected physical property changes due to structural modifications. In this work, we study $PtCl_4$ charge based doping.

However, the back-end-of-line processing of CNTs is not yet streamlined or CMOS compatible. CNTs require much higher temperature compared to Cu (up to 900 ^{o}C) [19] to achieve good quality CNT growth. Nevertheless, to achieve CMOS BEOL process compatibility, CNTs need to grow at lower temperatures such as 450 ^{o}C to 500 ^{o}C. However, at such temperatures CNTs have many defects, variations

This work was supported by the European Commission H2020 CONNECT project under grant agreement number 688612. (http://www.connect-h2020.eu/).

R. Chen, J. Liang, R. R. Pandey and A. Todri-Sanial are with the Microelectronics Department, LIRMM, University of Montpellier, CNRS, Montpellier, 34095 France. E-mails: rongmei.chen@lirmm.fr; aida.todri@lirmm.fr.

R. Ramos and J. Dijon are with the University Grenoble Alpes/CEA-LITEN, Grenoble, France.

J. Lee, V. P. Georgiev, and A. Asenov are with the School of Engineering, University of Glasgow, Glasgow, G12 8QQ UK.

H. Okuno and D. Kalita are with the University Grenoble Alpes/CEA-INAC, Grenoble, France.

S. Amoroso and C. Millar are with Synopsys, Ltd., Glasgow, UK.

Y. Cheng and L. Zhang are with the School of Electronic and Information Engineering, Beihang University, Beijing, China, 100191.

Manuscript submitted May 2018.

in diameter and chirality, which currently limit the practical application of CNTs as BEOL interconnects. Contacts are also a serious challenge for both reliability (good contact) and performance (high resistance). Metal electrodes might not be connected to all MWCNT shells, which detriments MWCNT interconnect performance.

While there is an extensive body of work on various methods for doping CNTs, there is not yet a systematic study of doping impact on MWCNT interconnects and their variability. Doping is capable of changing semiconducting CNTs into metallic CNTs concerning their electrical performance, and thus it is possible to reduce chirality variation and overall MWCNT resistance variation. In [20], we showed by atomistic-level simulation and experimental results how doping alters CNT chirality. However, there is still a need for further investigations to understand the impact of doping in the presence of various sources of variations such as defects, diameter, chirality, and connectivity.

In this work, we evaluate MWCNT interconnects performance and variability while considering the impact of doping. We introduce the parameter number of conducting channels (N_C) and incorporate it into our enhanced MWCNT compact model described in Part I. By theoretically calculating N_C as a function of Fermi level shift E_f - we evaluate each source of variation (diameter, chirality, defects) and all-sources using Monte Carlo (MC) simulations. Simulation results are subsequently compared with experimental results, and a good consistency is found between them. The contributions of our work can be summarized as follows.

1) We propose an analytical method for calculating N_C for metallic and semiconducting CNT shells and incorporate it into the compact model of MWCNT.
2) We perform MC simulations to study the impact of doping with different variations such as diameter, chirality, defects (defect density) and contacts. Finally, we assess the effectiveness of doping to mitigate the effects of process variations.
3) We present experimental results of MWCNT resistance before and after doping and compare them with simulation results. Good consistency is found between them, demonstrating the correctness of the simulation methodology and the proposed MWCNT compact model.

II. Analytical Method for Computing the Impact of Doping

Here, we present the analytical method for computing the impact of doping on N_C via the Fermi level shift E_f. The band structure of a zigzag CNT with chirality of (m, 0) can be described by Equation (1) [21]:

$$E(k_x) = \pm\frac{3ta_0}{2}\sqrt{k_x^2 + \left(\frac{1}{D_{CNT}}(2v - \frac{4}{3}m)\right)^2} \quad (1)$$

where D_{CNT} is the CNT diameter, k_x is the wave vector in the x direction, t is the hopping parameter, a_0 is the carbon-carbon distance, and v is an integer less than m. E_f is assumed to be 0.0 eV for pristine zigzag CNT although manufactured

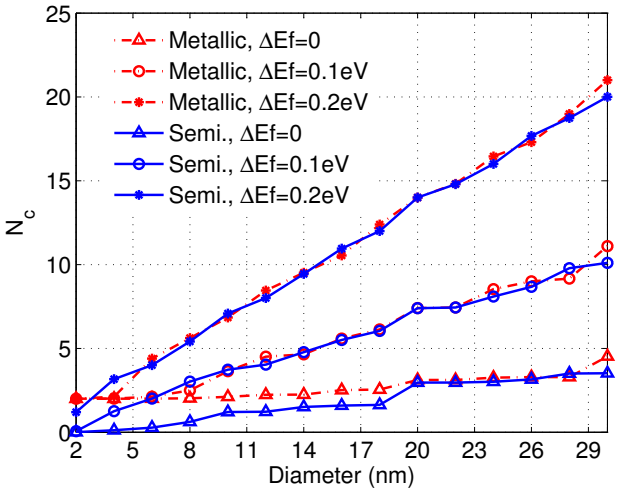

Fig. 1. Change of N_C with diameter for metallic and semiconducting CNTs before and after the E_f shift.

CNTs tend to be slightly p-doped by the oxygen in the air under ambient conditions [22] and have some downshift of E_f. From Equation (1), we can calculate the transmission coefficients ($T(E)$), and then N_C can be obtained as in Equation (2) [21]. It should be noted that the N_C of metallic armchair CNT can be calculated similarly [23].

$$N_C = \int T(E)f'(E, E_f)dE/(k_BT) \quad (2)$$

where f' is the derivative of the Fermi function, k_B is the Boltzmann constant, and T is the temperature. N_{Ci} of the CNT shell i in MWCNT modifies its intrinsic resistance R_i as Equations (3) and (4) [24] where $h/(2e^2) \sim 12.9$ kΩ and R_{Si}, R_Q and λ_i represent scattering and quantum resistances, and mean free path (MFP) of the CNT shell i, respectively. L is the MWCNT length.

$$R_i = R_Q + R_{Si}L = \frac{h}{2e^2N_{Ci}} + \frac{h}{2e^2N_{Ci}}\frac{L}{\lambda_i} \quad (3)$$

$$\lambda_i \approx 1000D_{CNT} \quad (4)$$

Calculated results for metallic and semiconducting CNTs of various diameters before and after the E_f shift are shown in Fig. 1. It shows that the increase in N_C is more significant for larger diameter CNTs than for smaller diameter CNTs. Moreover, metallic and semiconducting CNTs have almost the same N_C when their diameters are larger than 20 nm. The increase in N_C leads to increase in both conductance and quantum capacitance of MWCNT [24] and can change the performance of MWCNT interconnect.

In Fig. 2 we show the calculated results for different shells of an MWCNT with 11 nm outermost diameter. The negative shift of E_f corresponds to the p-type doping while the positive shift corresponds to the n-type doping. There are in total nine shells based on the shell number calculation equations (in Part I). The smallest or innermost diameter is 5.56 nm. Furthermore, we note from Fig. 2(c) that when E_f is shifted

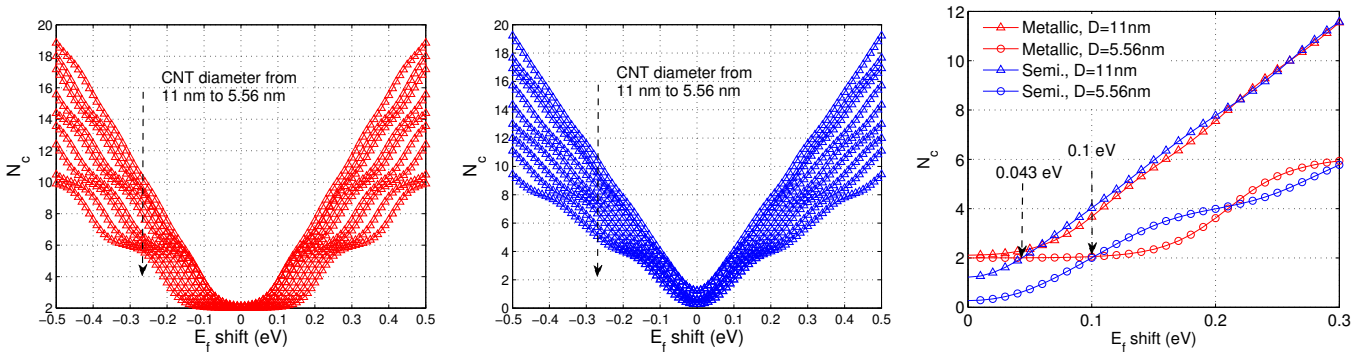

(a) Metallic shells for D_{max} = 11 nm MWCNT.

(b) Semiconducting shells for D_{max} = 11 nm MWCNT.

(c) D_{CNT}=11 nm and 5.56 nm shells.

Fig. 2. N_C of a) metallic shells with the E_f shift, b) N_C of semiconducting shells with the E_f shift for the MWCNT with 11 nm outermost diameter, and c) N_C of metallic and semiconducting shells of the outermost (11 nm) and the innermost (5.56 nm) shells before and after the E_f shift (similar for the negative E_f shift).

TABLE I
REPRESENTATIVE E_f SHIFTS FOR MWCNT WITH D_{max} = 11 NM AND THE N_C FOR METALLIC (N_{Cm}) AND SEMICONDUCTING (N_{Cs}) CNT SHELLS. ALSO SHOWN ARE THE RATIOS OF METALLIC CNT SHELLS AT DIFFERENT E_f SHIFTS.

E_f shifts (eV)	0	0.043	0.1	0.2	0.3
11 nm N_{Cs}	1.2	2.0	4.0	7.8	11.6
11 nm N_{Cm}	2.1	2.3	3.7	7.6	11.5
5.56 nm N_{Cs}	0.27	0.61	2.0	4.0	5.8
5.56 nm N_{Cm}	2.0	2.0	2.1	3.6	5.9
Metallic shell ratio after doping	1/3	1/3	1	1	1

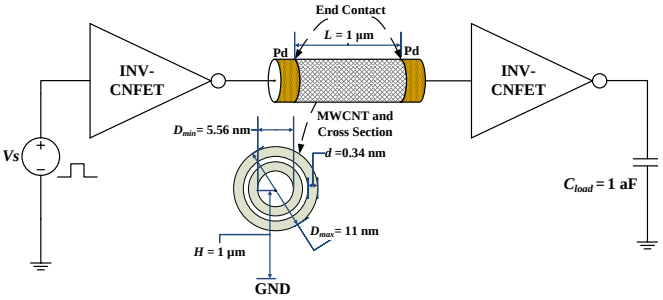

Fig. 3. Simulation setup schematic of MWCNT as interconnect. MWCNT is connected between two inverters composed of CNTFETs.

to 0.043 eV and 0.1 eV, the outermost and the innermost semiconducting CNT shells start to have N_C = 2, respectively.

Interestingly, pristine metallic CNTs also have N_C = 2 when their diameters are small ($\leq$ 11 nm, see Fig. 1). Hence, we deduce that a semiconducting CNT of a small diameter ($\leq$ 11 nm) becomes equivalent to a pristine metallic CNT when its N_C reaches 2 (N_C = 2) by shifting E_f. Additionally, we assume that the E_f shift is the same for both metallic and semiconducting CNT shells because no hint of doping selectivity for semiconducting and metallic CNTs is observed [4]. Furthermore, doping is assumed to have no impact on defect and contact resistance. Based on these assumptions and the simulations shown in Fig. 2(c), one can predict that a MWCNT with 11 nm outer diameter starts to degenerate semiconducting shells and increase metallic behavior when E_f is shifted by 0.043 eV with doping. All shells start behaving as metallic when E_f is shifted by 0.1 eV.

It is important to note that chirality which represents the carbon nanotube rotation angle does not change with doping - it is the N_C and electrical conductance of semiconducting shells that changes to metallic-like shell properties. Detailed information of N_C and the ratios of metallic CNT shells in the MWCNT at some specific E_f shifts are shown in Table I.

III. SIMULATION SETUP AND RESULTS

A. Simulation Setup

The simulation setup schematic is shown in Fig. 3, which is the same as in Part I of this paper. The circuit benchmark consists of two inverters connected through either an ideal wire or a MWCNT interconnect. Inverter gates are created with carbon nanotube field effect transistors (CNTFETs) based on compact models as in [25]. The key parameters of both n-type and p-type CNTFET are 11.7 nm, 1 μm, 10 nm for gate length, gate width and the distance between CNTs, respectively where other parameters are the default values recommended by [25]. We compute the MWCNT interconnect delay, power consumption, and power-delay product (PDP).

We conduct MC simulations for diameter, defects, chirality and all-sources variations. A detailed description of each variation source can be found in Part I of this paper. One thousand samples are collected to obtain a good confidence level for each simulation condition. We investigate MWCNT doping by considering the five representative E_f shifts as listed in Table I. For any given Fermi shift E_f (or doping concentration), the MWCNT compact model (described in Part I) is updated to take into account the N_C of each shell (either metallic or semiconducting). We also assume a defect density on each shell as 10 /μm.

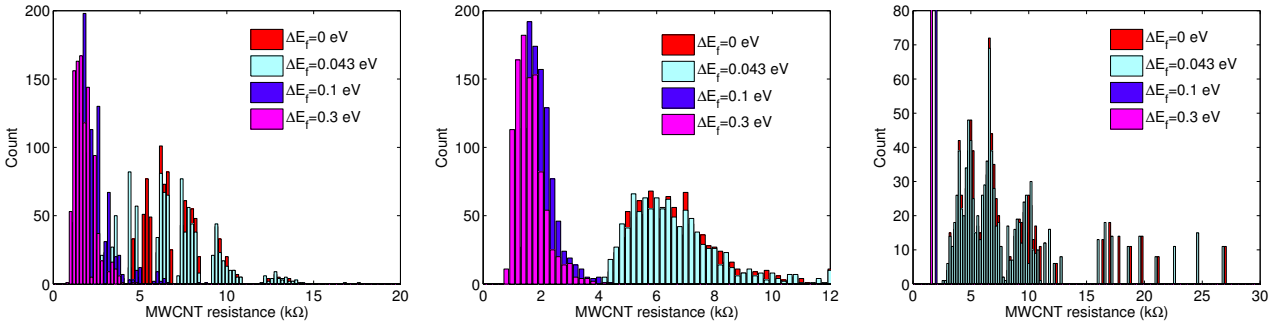

(a) Diameter (b) Defects (c) Chirality

Fig. 4. (a)-(c) are distributions of resistance variation of the MWCNT interconnect at different E_f shifts with input diameter, defects, and chirality variations respectively.

B. Impact of MWCNT Doping

In this work, we explore charge transfer doping as a means for reducing resistance variability. As described in Section II, doping shifts the E_f and introduces additional N_C for both metallic and semiconducting MWCNT shells (see Table I). We perform MC simulations for each source of variation (diameter, defects, and chirality) with different levels of E_f for doping. Results are shown in Fig. 4(a)-(c). The all-sources variation results are shown in Fig. 5. Foremost, we observe that doping lowers MWCNT resistance and narrows the distributions, particularly for the E_f shift from 0.043 eV to 0.1 eV. Similar trends are also obtained for MWCNT performance (delay, power, and PDP) and are not shown here.

We also calculated the mean value (μ), standard deviation (σ) and 3σ percentage ($3\sigma/\mu\times100\%$, used to estimate the largest possible percentage deviation from μ [26], [27]) of MWCNT resistance and performances with the E_f shift and are presented in Fig. 6 and Fig. 7(a)-(c), respectively for each source of variations. Based on our analytical method from Section II (Fig. 2(c)), we know that doping of $E_f \geq 0.043$ eV starts to increase N_C for metallic CNTs, whereas semiconducting CNTs begin to behave as metallic-like shells as $N_C \geq 2$. Hence, it is not until E_f reaches 0.043 eV that we start to observe improvements in MWCNT resistance and performances μ and σ as in Fig. 6. On the contrary, the σ and 3σ percentage of diameter variation increases to some extent when the E_f shift increases beyond 0.043 eV. This is because the outermost semiconducting shell of MWCNT at these E_f shifts can behave like metallic CNT shell when its diameter is larger than 11 nm as a result of diameter variation (see Table I and Fig. 1). The co-existence of metallic and semiconducting CNT shells makes the diameter variation more predominant. Due to the increase in diameter variation, the all-sources variation also slightly increases with E_f beyond 0.043 eV.

But, as E_f reaches 0.1 eV, all semiconducting shells behave as metallic, thus improving significantly MWCNT resistance μ and σ. As more doping is applied with E_f from 0.1 eV to

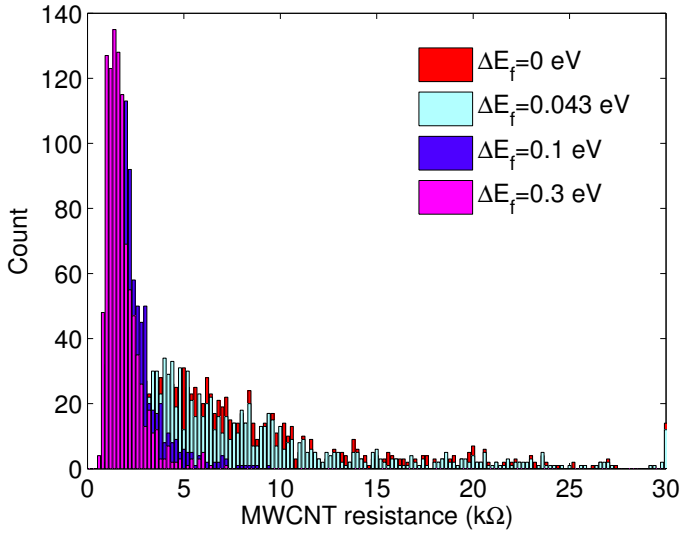

Fig. 5. Distributions of resistance variation of the MWCNT interconnect at different E_f shifts with input all-sources variation.

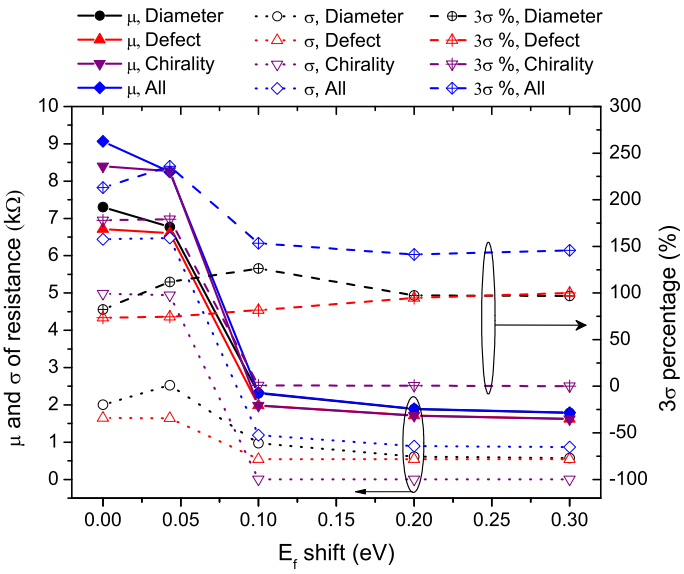

Fig. 6. Change of resistance of the MWCNT interconnect with the E_f shift for diameter, defect, chirality and all-sources variations.

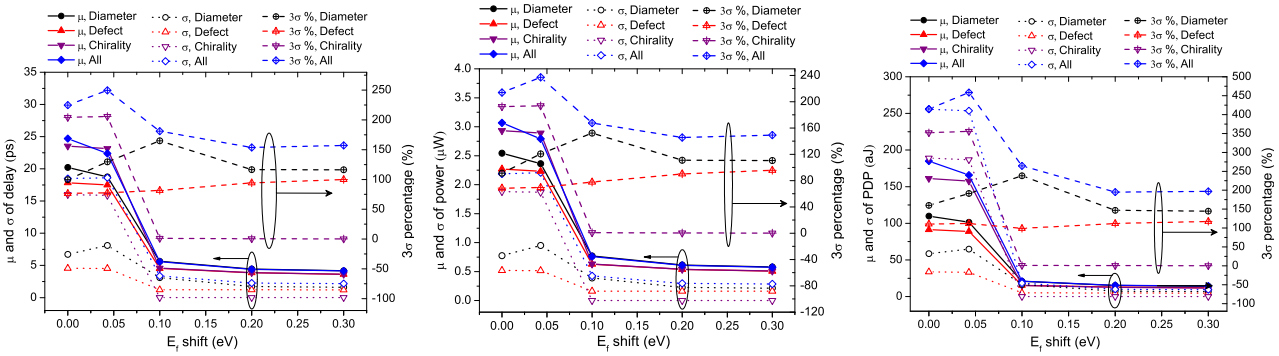

(a) Delay (b) Power (c) PDP

Fig. 7. (a)-(c) are change of delay, power and PDP variations of the MWCNT interconnect, respectively with the E_f shift for diameter, defect, chirality and all-sources variations.

0.3 eV, slight reductions in μ and σ are observed. This can be mainly explained due to two doping attributes: (1) significant CNT shell resistance reduction is obtained at E_f = 0.1 eV as all semiconducting shells behave as metallic shells, and (2) with more doping $E_f \geq$ 0.1 eV the N_C increases, however, resistance reductions is less drastic as in (1). Additionally, the change in the ratio of metallic to semiconducting CNT shells makes the chirality variation reduced (both σ and 3σ percentage). It approaches zero when E_f reaches 0.1 eV. We also note that although the σ of diameter and defects variation reduce with E_f of 0.1 eV, the 3σ percentage does not improve due to their similarly decreasing rate of μ. Both diameter and defect variations remain present as E_f shifts beyond 0.1 eV because they are not directly related to E_f or N_C and furthermore contact and defect resistances (contribute to diameter and defects variations) are assumed to be not impacted by doping in this work. Hence, their impact cannot be canceled out by doping.

All-sources variation shows a similar trend in resistance and performances σ to that of chirality variation with the E_f up to 0.1 eV as shown in Fig. 6 and 7. Beyond E_f of 0.1 eV, the contribution of chirality to overall variation is negligible, but the variations of diameter and defects dominate. We can deduce that doping helps to reduce overall MWCNT variation by decreasing the contribution of chirality variation mainly due to the degeneration of semiconducting shell properties to metallic. Doping has limited impact on defects and diameter (including contact resistance variation) variations, especially for the 3σ percentage variation.

C. Comparisons with Experimental Data

As described in [20], we developed a CNT integration process to grow individual MWCNTs at predefined locations on a silicon wafer by hot filament assisted CVD, and to individually contact them with Palladium (Pd) electrodes for electrical characterization. External doping of the MWCNT by $PtCl_4$ salt was then developed. To estimate the impact of doping under various conditions, similarly to [20], we assume the contact resistance is much smaller than MWCNT intrinsic resistance and compare the distributions of linear resistance before and after doping. In [20], a 40% reduction

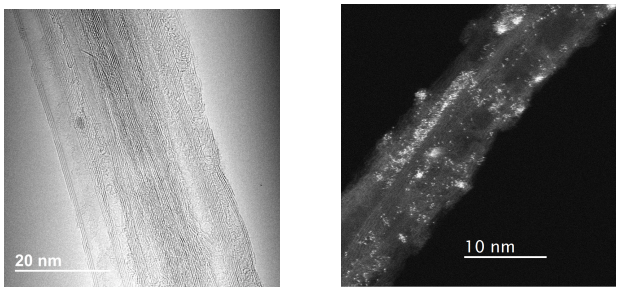

(a) Before doping (b) After doping

Fig. 8. TEM and STEM pictures for MWCNT before and after doping with $PtCl_4$, respectively.

TABLE II
COMPARISONS OF DOPING EFFICIENCY IN REDUCING MWCNT RESISTANCE BETWEEN THE ALL-SOURCES SIMULATION RESULTS AND THE EXPERIMENTAL DATA IN THIS WORK OR THAT FROM [20].

Doping process	Non doped	Dipping [20]	Spray dopant 1	Spray dopant 2
Estimated E_f shifts (eV)	0.00	0.104	0.122	0.250
σ, simulation	0%	-19.6%	-42.6%	-77.2%
σ, experiments	0%	-18.6%	-59.3%	-77.2%
μ, simulation	0%	-41.2%	-55.1%	-73.1%
μ, experiments	0%	-41.4%	-55.5%	-73.3%
3σ%, simulation	0%	38.9%	24.4%	-16.6%
3σ%, experiments	0%	39.0%	-8.5%	-14.5%

of the linear resistance was obtained by dipping the connected MWCNTs in $PtCl_4$ solution. In this work, we used a different doping process and instead sprayed the $PtCl_4$ solution on the connected MWCNTs to better control the amount of dopant on the CNTs. It is found that both mean value and variations of MWCNT resistance are significantly reduced after doping. In addition, higher doping efficiencies can be obtained with the spray doping process and that the Fermi level shift can be controlled by the amount of dopant deposited on the CNTs. TEM and STEM pictures of MWCNT before and after doping are shown in Fig. 8.

The measured average D_{max} of the experimentally doped MWCNTs was 6.5 nm. Because the defect density and MFP

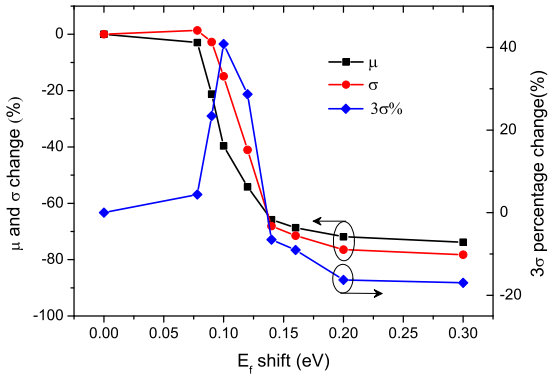

Fig. 9. Change of MWCNT resistivity and its variability from the all-sources simulation results with the E_f shift for the MWCNT of D_{max} = 6.5 nm (other parameters are the same to previous simulations).

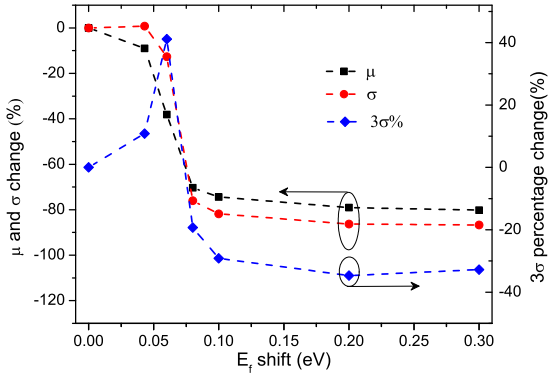

Fig. 10. Change of MWCNT resistivity and its variability from the all-sources simulation results with the E_f shift for MWCNT of D_{max} = 11 nm (MFP = $1000D_{CNT}$).

of these doped CNTs are not measurable, direct comparisons of μ and σ of MWCNT resistance between experiments and simulation (all-sources variation) are difficult and meaningless. Instead, we compare relative change (or doping efficiency) in MWCNT resistance μ and σ, and the 3σ percentage variations with E_f shift for MWCNTs of D_{max} = 6.5 nm. Fig. 9 shows the simulation results of MWCNT doping efficiency with E_f shift. In Table II, we show doping efficiency of μ and σ, and 3σ percentage variations before and after doping for experimental results (obtained this work or those from [20]). By comparing these simualtion reuslts and experimental results we can further predict the Fermi shift due to experimental doping, as presented in the table. For comparisons, the corresponding μ, σ and 3σ relative percentage reductions from Fig. 9 are shown in Table II as well. The most significant deviation between the simulation results and experimental data is the relative change in 3σ percentage variation at the E_f shift of 0.122 eV. This can be attributed to the abrupt change in 3σ percentage variation as shown in Fig. 9 and the assumed E_f = 0 eV for pristine CNTs (before doping operation) which may be incorrect because p-doped CNTs have an E_f downshift which can be expected during fabrication [4], [22].

Except for the 3σ percentage deviation, an overall good match between experimental data and simulation results is observed, which strongly demonstrates the capability of the

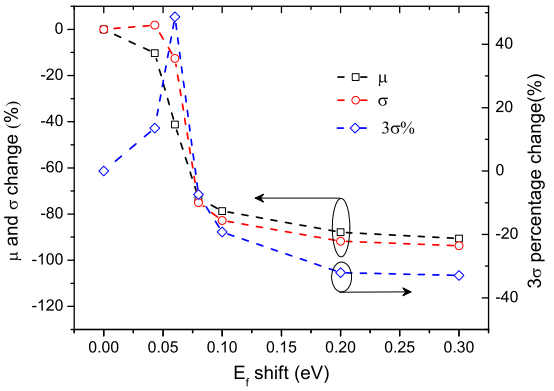

Fig. 11. Change of MWCNT resistivity and its variability from the all-sources simulation results with E_f shift for MWCNT of D_{max} = 11 nm (MFP = $10D_{CNT}$).

MWCNT compact model to quantitatively predict relative change in MWCNT performance and the doping efficiency.

D. Doping Efficiency

1) Impact of MWCNT diameter: It is worth noting that the required level of the E_f shift (or effective E_f shift) to achieve a significant improvement of MWCNT resistance is dependent on the MWCNT dimensions though the overall change of doping efficiency with doping is similar. For example, by decreasing D_{max} from 11 nm to 6.5 nm, the effective E_f shift is increased from $\sim$ 0.1 eV to $\sim$ 0.16 eV but the overall change of doping efficiency with doping is similar, as shown in Fig. 9 and Fig. 10.

2) Impact of MFP: CNTs are of interest due to their ballistic transport and long mean free path (MFP). In this work, we assume that the default value of MFP in each shell of MWCNT is 1000 times the CNT shell diameter [24]. However, MFP is dependent on MWCNT fabrication process and thus may change from process to process. For instance, based on the scattering resistance of CVD-grown MWCNTs measured in [20] and in this work - it appears that MFP is shorter than 100 nm ($\sim$10-20 $\times$ D_{CNT}), which is also in agreement with other literature reports [28]. So, it is worth investigating the impact of MFP on doping efficiency by considering different MFPs. Simulation results of doping efficiency for MFP of 10 $\times$ D_{CNT} are presented in Fig. 11 and compared with the default case (MFP of 1000 $\times$ D_{CNT}) in Fig. 10. It shows that despite the 100 times difference in MFP, doping efficiency is similar. This is because doping increases N_C of CNT shells and further improves conductance of MWCNT, which is impacted by MFP proportionally under different N_C as shown in Equations (3) and (4). As a result, we deduce that the MFP does not impact the relative change of MWCNT resistance and performance improvements obtained from doping.

3) Impact of Pristine MWCNT chirality: As demonstrated in Section III-B, the improvement of MWCNT performance and variability with doping is mainly attributed to chirality variation reduction. Because the chirality variation results from the change of metallic and semiconducting CNT shell portions, it is reasonable to deduce that the doping efficiency can be

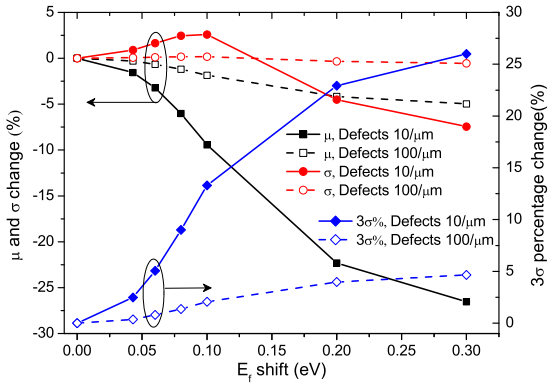

Fig. 12. Change of metallic MWCNT resistivity and its variability from the all-sources simulation results with the E_f shift for defect density of 10 /μm (the default) and 100 /μm.

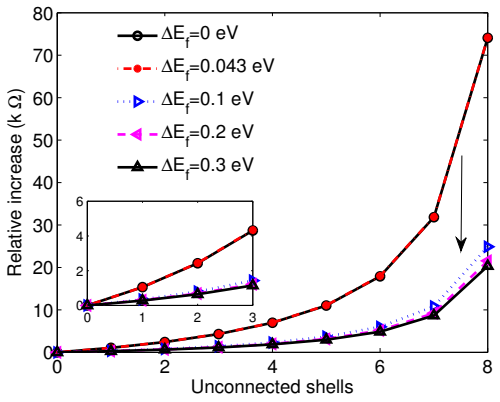

Fig. 13. Relative increase in the worst case MWCNT delay with several disconnected shells and E_f shift levels compared to the case of all (nine) connected shells. The inset is the simulation result of unconnected shells from 0 to 3 after zooming in.

degraded if the original MWCNT is more metallic, namely a larger portion of metallic CNT shells. For example, Fig. 12 shows the simulation results of entirely metallic MWCNT, namely metallic chirality 1 (other parameters are the same as the default one) with the E_f shift. Compared with the default MWCNT (1/3 of metallic CNT shells) as shown in Fig. 10, the doping efficiency is reduced for the entirely metallic MWCNT. Instead of the abrupt reduction in μ and σ of MWCNT resistance for the default MWCNT from the E_f shift of 0.043 eV to 0.1 eV, a continuous and slow reduction is observed for the entirely metallic MWCNT up to 0.3 eV. Moreover, different from the default case where 3σ percentage can finally be reduced by doping up to 0.1 eV, the 3σ percentage is continuously increased with doping for the entire metallic MWCNT case.

4) Impact of Defect Density: We study the impact of defect density and in Fig. 12 we show the simulation results of doping efficiency for the entire metallic MWCNT. We observe that with the increase in defect density, doping effectiveness is significantly reduced for the entire metallic MWCNT. For example, the doping efficiency of μ and σ of MWCNT resistance at the 0.3 eV E_f shift is 26.5%/7.3% and 5.0%/0.7% for defect density of 10 /μm and 100 /μm, respectively. The 3σ percentage is increased relatively by 26.1% and 4.5%, respectively. This is because the role of diameter and defect variations are relatively more important as defect density is increased for the case of entirely metallic MWCNT. However, it is found that for the default case of 1/3 metallic chirality, the defect density impact on doping effectiveness is negligible (less than 2% and 4% difference are observed at the E_f of 0.1 eV and 0.3 eV, respectively). This is due to the dominant impact of chirality variation to the overall variation response with E_f shift for the default case.

E. MWCNT Shell to Contact Variations

Here, we study the impact of doping on MWCNT shells connectivity to contact. In Fig. 13, we show the relative worst case (the outermost shells disconnected, as discussed in Part I of this paper) resistance degradation (similar to σ) versus a different number of disconnected shells for different E_f shift levels compared to all shells connected case. No significant improvements with doping are observed till E_f = 0.043 eV and significant improvements are observed for $E_f \geq$ 0.1 eV. When normalizing the relative worst resistance degradation to the case with all shells connected resistance (similar to σ/μ, namely relative variation), it is found that there is not an obvious impact from doping up to five disconnected shells (out of nine shells total) and increases slightly as more shells are disconnected. MWCNTs performances with disconnected shell have a similar response to doping and are not shown here. Hence, we deduce that doping improves MWCNT resistance and then performances, which allows mitigating the effect of disconnected shells without increasing relative variation significantly.

IV. Discussion and Conclusion

In this work, we show that by doping (E_f shift to 0.1 eV) on a MWCNT of D_{max} = 11 nm significant improvements on performance and variability can be obtained. However, we also show that for MWCNT of smaller diameters, more doping or E_f shift is required to achieve these improvements. Hence, as technology scales, the local interconnect sizes also decrease [29], which implies that MWCNT interconnects for advanced technology node applications may need higher doping levels to improve their performance and variability efficiently. Moreover, the N_C of semiconducting CNT shells decrease with their diameter and technology scaling, hence, increasing the importance of applying doping to local interconnects with small geometries to improve MWCNT resistance and chirality variation. However, doping can do much. Other sources of variations such as diameter and defects will require further improvement on CNT process growth to exploit the potentials of MWCNTs for interconnect application.

In this work, we propose an enhanced compact model for MWCNT interconnects to take into account variability including diameter, defects, chirality and connectivity but also the impact of doping as a countermeasure to large resistance variability. Based on the analytical formulations, the change

of MWCNT resistance and performance variation (including delay, power, and PDP) with E_f shift can be calculated while including variations on diameter, defect densities, chirality, and shell-to-contact connectivity. We identify that chirality variation (both σ and 3σ percentage) can be significantly reduced to almost zero when the doping E_f shift enables to degenerate all semiconducting shells to equivalent metallic like shell conductivity. Also, the diameter and defect variations σ can be reduced up to $\sim$80% while the 3σ percentage is slightly increased. The efficiency of doping is compared with experimental data, and an overall good match is obtained, which demonstrates the validity of computing doping efficiency and simulation methodology. We observe that MFP has a minor effect on doping efficiency. However, doping efficiency can be significantly reduced and degraded if the original portion of metallic CNT shells increases. Overall, we have established the analytical methods and simulation framework to study charge based doping impact on MWCNT interconnects performance and variability.

ACKNOWLEDGMENT

This project has received funding from the European Unions Horizon 2020 research and innovation program under grant agreement No 688612. (http://www.connect-h2020.eu/).

REFERENCES

[1] A. Todri-Sanial, J. Dijon, and A. Maffucci, *Carbon Nanotubes for Interconnects*. Springer, 2017 ISBN: 978-3-319-29744-6. doi: 10.1007/978-3-319-29746-0

[2] K. Liew, C. Wong, X. He, and M. Tan, "Thermal stability of single and multi-walled carbon nanotubes," *Physical Review B*, vol. 71, no. 7, p. 075424, 2005. doi: 10.1103/physrevb.71.075424

[3] B. Wei, R. Vajtai, and P. Ajayan, "Reliability and current carrying capacity of carbon nanotubes," *Applied Physics Letters*, vol. 79, no. 8, pp. 1172–1174, 2001. doi: 10.1063/1.1396632

[4] W. Zhou, J. Vavro, N. M. Nemes, J. E. Fischer, F. Borondics, K. Kamaras, and D. Tanner, "Charge transfer and fermi level shift in p-doped single-walled carbon nanotubes," *Physical Review B*, vol. 71, no. 20, p. 205423, 2005. doi: 10.1103/physrevb.71.205423

[5] J. Liang, L. Zhang, N. Azemard-Crestani, P. Nouet, and A. Todri-Sanial, "Physical description and analysis of doped carbon nanotube interconnects," *IEEE International Workshop on Power and Timing Modeling, Optimization and Simulations (PATMOS)*, pp. 250–255, 2016. doi: 10.1109/patmos.2016.7833695

[6] M. Monthioux, *Carbon meta-nanotubes: Synthesis, properties and applications*. John Wiley & Sons, 2011. doi: 10.1002/9781119954743

[7] L. Yu, C. Shearer, and J. Shapter, "Recent development of carbon nanotube transparent conductive films," *Chemical reviews*, vol. 116, no. 22, pp. 13 413–13 453, 2016. doi: 10.1021/acs.chemrev.6b00179

[8] S. L. Hellstrom, M. Vosgueritchian, R. M. Stoltenberg, I. Irfan, M. Hammock, Y. B. Wang, C. Jia, X. Guo, Y. Gao, and Z. Bao, "Strong and stable doping of carbon nanotubes and graphene by moo x for transparent electrodes," *Nano letters*, vol. 12, no. 7, pp. 3574–3580, 2012. doi: 10.1021/nl301207e

[9] B. Chandra, A. Afzali, N. Khare, M. M. El-Ashry, and G. S. Tulevski, "Stable charge-transfer doping of transparent single-walled carbon nanotube films," *Chemistry of Materials*, vol. 22, no. 18, pp. 5179–5183, 2010. doi: 10.1021/cm101085p

[10] J. E. Fischer, "Chemical doping of single-wall carbon nanotubes," *Accounts of chemical research*, vol. 35, no. 12, pp. 1079–1086, 2002. doi: 10.1021/ar0101638

[11] L. Kavan, P. Rapta, L. Dunsch, M. J. Bronikowski, P. Willis, and R. E. Smalley, "Electrochemical tuning of electronic structure of single-walled carbon nanotubes: in-situ raman and vis-nir study," *The Journal of Physical Chemistry B*, vol. 105, no. 44, pp. 10 764–10 771, 2001. doi: 10.1021/jp011709a

[12] J. Kong, N. R. Franklin, C. Zhou, M. G. Chapline, S. Peng, K. Cho, and H. Dai, "Nanotube molecular wires as chemical sensors," *science*, vol. 287, no. 5453, pp. 622–625, 2000. doi: 10.1126/science.287.5453.622

[13] V. Skakalova, A. Kaiser, U. Dettlaff-Weglikowska, K. Hrncarikova, and S. Roth, "Effect of chemical treatment on electrical conductivity, infrared absorption, and raman spectra of single-walled carbon nanotubes," *The Journal of Physical Chemistry B*, vol. 109, no. 15, pp. 7174–7181, 2005. doi: 10.1021/jp044741o

[14] B. B. Parekh, G. Fanchini, G. Eda, and M. Chhowalla, "Improved conductivity of transparent single-wall carbon nanotube thin films via stable postdeposition functionalization," *Applied Physics Letters*, vol. 90, no. 12, p. 121913, 2007. doi: 10.1063/1.2715027

[15] Y. Zhao, J. Wei, R. Vajtai, P. M. Ajayan, and E. V. Barrera, "Iodine doped carbon nanotube cables exceeding specific electrical conductivity of metals," *Scientific reports*, vol. 1, p. 83, 2011. doi: 10.1038/srep00083

[16] S. Esconjauregui, L. DArsie, Y. Guo, J. Yang, H. Sugime, S. Caneva, C. Cepek, and J. Robertson, "Efficient transfer doping of carbon nanotube forests by moo3," *ACS nano*, vol. 9, no. 10, pp. 10 422–10 430, 2015. doi: 10.1021/acsnano.5b04644

[17] J. Dijon, R. Ramos, A. Fournier, H. Le Poche, H. Fournier, H. Okuno, and J. Simonato, "Record resistivity of in-situ grown horizontal carbon nanotube interconnect," in *Technical proceedings of the 2014 NSTI nanotechnology conference and expo, NSTI-Nanotech*, vol. 3, 2014, pp. 17–20. [Online]. Available: https://www.nsti.org/procs/Nanotech2014v3/1/T2.154

[18] B. Padya, D. Kalita, P. Jain, G. Padmanabham, M. Ravi, and K. Bhat, "Self-organized growth of bamboo-like carbon nanotube arrays for field emission properties," *Applied Nanoscience*, vol. 2, no. 3, pp. 253–259, 2012. doi: 10.1007/s13204-012-0102-z

[19] A. L. P. L. P. Petit, S. Roche, and J. Salvetat, *Understanding Carbon Nanotubes, from Basics to Application*. Lect. Notes Phys., édition Springer, 2006. doi: 10.1007/b10971390

[20] J. Liang, R. Ramos, J. Dijon, H. Okuno, D. Kalita *et al.*, "A physics-based investigation of pt-salt doped carbon nanotubes for local interconnects," in *Electron Devices Meeting (IEDM), 2017 IEEE International*. IEEE, 2017, pp. 35–5. doi: 10.1109/iedm.2017.8268502

[21] H. H. B. Sørensen, P. C. Hansen, D. E. Petersen, S. Skelboe, and K. Stokbro, "Efficient wave-function matching approach for quantum transport calculations," *Physical Review B*, vol. 79, no. 20, p. 205322, 2009. doi: 10.1103/physrevb.79.205322

[22] X. Ma, L. Adamska, H. Yamaguchi, S. E. Yalcin, S. Tretiak, S. K. Doorn, and H. Htoon, "Electronic structure and chemical nature of oxygen dopant states in carbon nanotubes," *ACS nano*, vol. 8, no. 10, pp. 10 782–10 789, 2014. doi: 10.1021/nn504553y

[23] S. Datta, *Quantum transport: atom to transistor*. Cambridge university press, 2005. doi: 10.1017/cbo9781139164313

[24] H. Li, W.-Y. Yin, K. Banerjee, and J.-F. Mao, "Circuit modeling and performance analysis of multi-walled carbon nanotube interconnects," *IEEE Transactions on electron devices*, vol. 55, no. 6, pp. 1328–1337, 2008. doi: 10.1109/ted.2008.922855

[25] C.-S. Lee, E. Pop, A. D. Franklin, W. Haensch, and H.-S. Wong, "A compact virtual-source model for carbon nanotube fets in the sub-10-nm regimepart i: Intrinsic elements," *IEEE transactions on electron devices*, vol. 62, no. 9, pp. 3061–3069, 2015. doi: 10.1109/ted.2015.2457453

[26] A. Nieuwoudt and Y. Massoud, "On the impact of process variations for carbon nanotube bundles for vlsi interconnect," *IEEE Transactions on Electron Devices*, vol. 54, no. 3, pp. 446–455, 2007. doi: 10.1109/ted.2006.890364

[27] F. Pukelsheim, "The three sigma rule," *The American Statistician*, vol. 48, no. 2, pp. 88–91, 1994. doi: 10.1080/00031305.1994.10476030

[28] A. A. Vyas, C. Zhou, and C. Y. Yang, "On-chip interconnect conductor materials for end-of-roadmap technology nodes," *IEEE Transactions on Nanotechnology*, 2016. doi: 10.1109/tnano.2016.2635583

[29] L. Wilson, "International technology roadmap for semiconductors (itrs)," *Semiconductor Industry Association*, 2013. [Online]. Available: http://www.itrs2.net/2013-itrs.html